



 Cite this: *RSC Adv.*, 2019, 9, 519

# Molybdenum imidazole citrate and bipyridine homocitrate in different oxidation states – balance between coordinated $\alpha$ -hydroxy and $\alpha$ -alkoxy groups†

 Si-Yuan Wang and Zhao-Hui Zhou \*

Oxo and thiomolybdenum(IV/VI) imidazole hydrocitrate  $K_2\{Mo_3^{IV}O_4(im)_3[Mo^{VI}O_3(Hcit)]_2\} \cdot 3im \cdot 4H_2O$  (**1**),  $(Him)_2\{Mo_3^{IV}SO_3(im)_3[Mo^{VI}O_3(Hcit)]_2\} \cdot im \cdot 6H_2O$  (**2**), molybdenum(V) bipyridine homocitrate *trans*- $[(Mo^{VO})_2O(H_2homocit)_2(bpy)_2] \cdot 4H_2O$  (**3**) and molybdenum(VI) citrate  $(Et_4N)[Mo^{VI}O_2Cl(H_2cit)] \cdot H_2O$  (**4**) ( $H_4cit$  = citric acid,  $H_4homocit$  = homocitric acid, *im* = imidazole and *bpy* = 2,2'-bipyridine) with different oxidation states were prepared. **1** and **2** are the coupling products of  $[Mo^{VI}O_3(Hcit)]^{3-}$  anions and incomplete cubane units  $[Mo_3^{IV}O_4]^{4+}$  ( $[Mo_3^{IV}SO_3]^{4+}$ ) with monodentate imidazoles, respectively, where tridentate citrates coordinate with  $\alpha$ -hydroxy,  $\alpha$ -carboxy and  $\beta$ -carboxy groups, forming pentanuclear skeleton structures. The molybdenum atoms in **1** and **2** show unusual +4 and +6 valences based on charge balances, theoretical bond valence calculations and Mo XPS spectrum. The coordinated citrates in **1** and **2** are protonated with  $\alpha$ -hydroxy groups, while **3** and **4** with higher oxidation states of +5 and +6 are deprotonated with  $\alpha$ -alkoxy group even under strong acidic condition, respectively. This shows the relationship between the oxidation state and protonation of the  $\alpha$ -alkoxy group in citrate or homocitrate, which is related to the protonation state of homocitrate in FeMo-cofactor of nitrogenase. The homocitrate in **3** chelates to molybdenum(V) with bidentate  $\alpha$ -alkoxy and monodentate  $\alpha$ -carboxy groups. Molybdenum(VI) citrate **4** is only protonated with coordinated and uncoordinated  $\beta$ -carboxy groups. The solution behaviours of **1** and **2** are discussed based on  $^1H$  and  $^{13}C$  NMR spectroscopies and cyclic voltammograms, showing no decomposition of the species.

 Received 4th November 2018  
Accepted 11th December 2018

DOI: 10.1039/c8ra09134j

[rsc.li/rsc-advances](http://rsc.li/rsc-advances)

## Introduction

Molybdenum is widely present in water, soil, various animals and plants, and constitutes a variety of metalloenzymes with redox functions.<sup>1,2</sup> Homocitrate as a chelating ligand bound to  $Mo^{IV/III}$  of FeMo-cofactor plays a critical role in nitrogen fixation.<sup>3–11</sup> Homocitric acid is also a key intermediate in the biosynthetic pathway to the essential amino acid lysine in fungi and euglenids.<sup>12–14</sup> Molybdenum homocitrate is also considered to be involved in the final biosynthesis of FeMo-cofactor by the coupling reaction with iron clusters.<sup>15,16</sup> *R*-Homocitrate, whose long and flexible  $CH_2CO_2$  arm can form a hydrogen bond with the NH group of the imidazole ligand, may play an important role in the process of reducing nitrogen.<sup>17,18</sup> The source and path of protons in homocitrate have been an important topic in nitrogenase.<sup>19–25</sup>

As a homolog of homocitrate, citrate is also a complexing agent used in the preparations of Co(Ni)–Mo catalyst precursors of hydrosulfurization or baths for the electrodeposition of molybdenum–iron metal alloys, which assure a stable pH value during the deposition process in the electrolyte.<sup>26–31</sup> Molybdenum citrate has also been discovered in *nifV* nitrogenase and the sensor kinase *CitA*.<sup>32,33</sup> The incomplete cuboidal clusters  $Mo_3S_4$ ,  $Mo_3S_3O$ ,  $Mo_3SO_3$  and  $Mo_3O_4$  can form complexes with various types of ligands as a classic low-valence Mo skeleton structure,<sup>34–43</sup> which exists in Mo storage protein.<sup>44</sup> The latter also contains octanuclear molybdenum complexes  $[Mo_8O_{26}(im)_2]^{4-}$  with imidazole from histidine residue as polyoxometalates.<sup>44–46</sup>

It is noted that most of the mixed-valence molybdenum complexes are in  $VI/V$  and  $V/IV$ ,<sup>47–54</sup> while molybdenum( $VI/IV$ ) complex is less common.<sup>55</sup> Here two pentanuclear imidazole hydrocitrate molybdenum( $VI/IV$ ) complexes  $K_2\{Mo_3^{IV}VO_4(im)_3[Mo^{VI}O_3(Hcit)]_2\} \cdot 3im \cdot 4H_2O$  (**1**) and  $(Him)_2\{Mo_3^{IV}SO_3(im)_3[Mo^{VI}O_3(Hcit)]_2\} \cdot im \cdot 6H_2O$  (**2**) have been obtained with protonated  $\alpha$ -hydroxy groups, while dimeric bipyridine oxomolybdenum(V) homocitrate *trans*- $[(Mo^{VO})_2O(H_2homocit)_2(bpy)_2] \cdot 4H_2O$  (**3**) and mononuclear oxomolybdenum(VI) hydrocitrate  $(Et_4N)[Mo^{VI}O_2Cl(H_2cit)] \cdot H_2O$  (**4**) were captured with coordinate  $\alpha$ -alkoxy groups in acidic solution.

State Key Laboratory for Physical Chemistry of Solid Surfaces, College of Chemistry and Chemical Engineering, Xiamen University, Xiamen, 361005, China. E-mail: zhzhou@xmu.edu.cn; Fax: +86-592-2183047; Tel: +86-592-2184531

† Electronic supplementary information (ESI) available: IR, UV-Vis, NMR, XPS, CV and mass spectra. CCDC 1571186 and 1837477–1837479. For ESI and crystallographic data in CIF or other electronic format see DOI: 10.1039/c8ra09134j



## Results and discussion

Until now, a number of citrate or imidazole molybdenum complexes have been reported, while there is less interest on the mixed-ligand complexes of citrate and imidazole.<sup>45,47,56–59</sup> Most of the mixed-valence molybdenum complexes focus on Mo(vi)/Mo(v) and Mo(v)/Mo(iv),<sup>47–54</sup> fewer examples of Mo(vi)/Mo(iv) have been reported.<sup>55</sup> Here pentanuclear molybdenum(iv/vi) imidazole hydrocitrates  $K_2\{Mo_3^{IV}O_4(im)_3[Mo^{VI}O_3(Hcit)]_2\} \cdot 3im \cdot 4H_2O$  (**1**) and  $(Him)_2\{Mo_3^{IV}SO_3(im)_3[Mo^{VI}O_3(Hcit)]_2\} \cdot im \cdot 6H_2O$  (**2**) were obtained from an aqueous solution. The valences of the molybdenum atoms in **1** and **2** are +4 or +6 based on the charge balances, theoretical bond valence calculations and Mo XPS spectrum, which will be discussed later. They are different from the common mixed-valence complexes in the adjacent valence state, which are coordinated with citrate and imidazole.<sup>47,60</sup>

Increasing the temperature can enhance the coordination abilities of citric acid and imidazole. High-valent molybdenum atoms are reduced in a closed Teflon-lined stainless steel container with the aid of a reducing agent. Low-valent molybdenum atoms and weak alkaline conditions can avoid the protonation of imidazole, making it easier for coordination with molybdenum citrate simultaneously. Possible routes for molybdenum citrates **1**, **2** and **4** are outlined in Scheme 1 in three steps. First, the molybdates are reduced to tetravalent molybdenum cations  $[Mo_3^{IV}O_4(H_2O)_9]^{4+}$  or  $[Mo_3^{IV}SO_3(H_2O)_9]^{4+}$  respectively.<sup>61</sup> The imidazoles as monodentate ligands

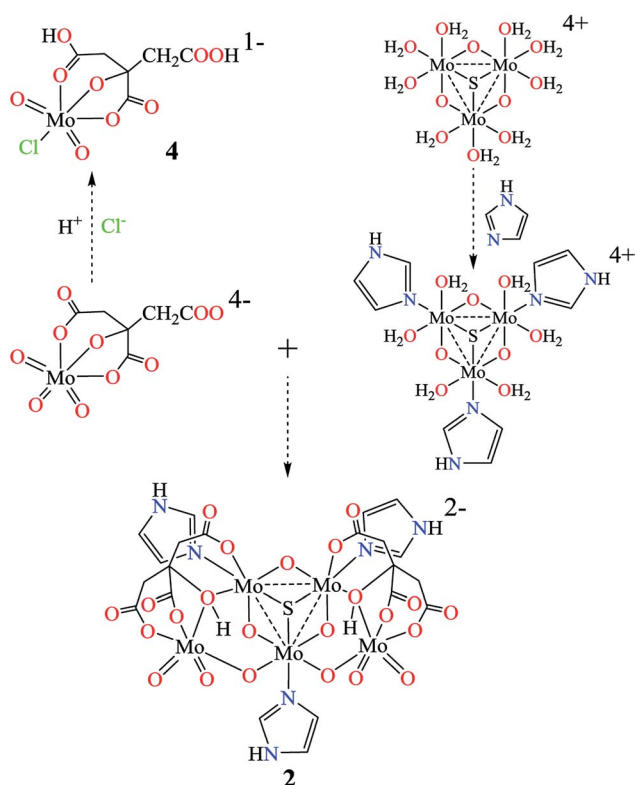
coordinate to the molybdenum(iv) atoms in  $[Mo_3^{IV}O_4(H_2O)_9]^{4+}$  or  $[Mo_3^{IV}SO_3(H_2O)_9]^{4+}$  ions. Free  $\beta$ -carboxy and  $\alpha$ -alkoxy groups in  $[Mo^{VI}O_3(cit)]^{4-}$  further coordinate with the molybdenum atom(iv) atoms in  $[Mo_3^{IV}O_4(H_2O)_9]^{4+}$  ion, forming a pentanuclear structure  $\{Mo_3^{IV}O_4(im)_3[Mo^{VI}O_3(Hcit)]_2\}^{2-}$  with  $\alpha$ -hydroxy groups. When  $Na_2S_2O_4$  was used instead of hydrazine dihydrochloride as a reducing agent, the  $\mu_3$ -O of  $[Mo_3^{IV}O_4]^{4+}$  in **1** is replaced by  $\mu_3$ -S to form  $[Mo_3^{IV}SO_3]^{4+}$ . Moreover, one of the terminal oxygen in  $[Mo^{VI}O_3(H_2cit)]^{2-}$  could be replaced by chloride under strong acidic conditions. The  $[Mo^{VI}O_2Cl(H_2cit)]^-$  ion was further captured by the large cation  $(Et_4N)^+$  as **4** without protonation in  $\alpha$ -alkoxy group.

Previously, a series of molybdenum(vi) homocitrates have been synthesized.<sup>62–65</sup> The strong chelating agent, 2,2'-bipyridine, assisted the formation of reduced molybdenum(v) homocitrate *trans*- $[(Mo^V)_2O(H_2homocit)_2(bpy)_2] \cdot 4H_2O$  (**3**) in the presence of hydrazine. The insoluble complex **3** crystallized immediately with a decrease in temperature. Attempts to prepare molybdenum(iv) homocitrate and molybdenum(iv/vi) imidazole homocitrate were not yet successful.

As shown by the X-ray crystal structures (Fig. 1 and S1–S4<sup>†</sup>),  $K_2\{Mo_3^{IV}O_4(im)_3[Mo^{VI}O_3(Hcit)]_2\} \cdot 3im \cdot 4H_2O$  (**1**) and  $(Him)_2\{Mo_3^{IV}SO_3(im)_3[Mo^{VI}O_3(Hcit)]_2\} \cdot im \cdot 6H_2O$  (**2**) are pentanuclear imidazole hydrocitrato molybdenum(iv/vi) complexes. An incomplete cubane cluster anion  $[Mo_3^{IV}O_4]^{4+}$  or  $[Mo_3^{IV}SO_3]^{4+}$  in **1** or **2** is joined by imidazole to form the circular species, respectively. Each molybdenum atom(iv) is surrounded octahedrally by two  $\mu_2$ -O, one  $\mu_3$ -O/S and one N atom of the imidazole ligand. The three imidazole ligands occupy a *cis* position to the  $\mu_2$ -O. This is similar to the reported  $Mo_3O_4(his)_3$  cluster in the Mo storage protein with an incomplete cubane anion, where each molybdenum atom is octahedrally coordinated to five O atoms and to the imidazole  $N_{E2}$  atom of  $his\alpha 140$ .<sup>44</sup> Moreover, molybdenum(vi) atoms in **1** or **2** are hexa-coordinated in approximate octahedral geometries respectively. The citrate ligand uses its  $\alpha$ -hydroxy,  $\alpha$ -carboxy and one  $\beta$ -carboxy groups to act as a tridentate ligand. The other  $\beta$ -carboxy and  $\alpha$ -hydroxy groups of the citrate further coordinate with the other molybdenum atom(iv). Each molybdenum(vi) citrate connects to  $[Mo_3^{IV}O_4]^{4+}$  or  $[Mo_3^{IV}SO_3]^{4+}$  unit with an O- or S-bridge to constitute novel pentanuclear skeleton structures.<sup>15</sup>

Hydrogen bonds of the imidazoles played important roles in the crystal packing of **1** and **2** (Fig. S5–S8, Tables S1 and S2<sup>†</sup>). The free imidazole as well as the imidazole ligand can act as providers for the two types of hydrogen bonds as N–H $\cdots$ O and N–H $\cdots$ N. N–H $\cdots$ O interactions, which are found in imidazole with bridging or terminal oxygen atoms, and oxygen atoms from citrate or water molecules. Hydrogen bonds in the form of N–H $\cdots$ N are only observed in **1**.

*Trans*- $[(Mo^V)_2O(H_2homocit)_2(bpy)_2] \cdot 4H_2O$  (**3**) is dimeric bipyridine homocitrato oxomolybdenum(v) complex as shown in Fig. 2 and S9.<sup>†</sup> Mo atoms in **3** are hexacoordinate in distorted geometries and surrounded octahedrally by one  $\mu_2$ -O, one terminal O, two O atoms of homocitrate and two N atoms of 2,2'-bipyridine. The homocitrate anions chelate to the Mo *via*  $\alpha$ -alkoxy and monodentate  $\alpha$ -carboxy groups, while the  $\beta$ - and  $\gamma$ -carboxylic acidic groups remain free. The homocitrate



Scheme 1 Possible routes for molybdenum(iv/vi) imidazole hydrocitrates **1** and **2** and ( $\mu_3$ -X = S or O) molybdenum(vi) citrate **4**.



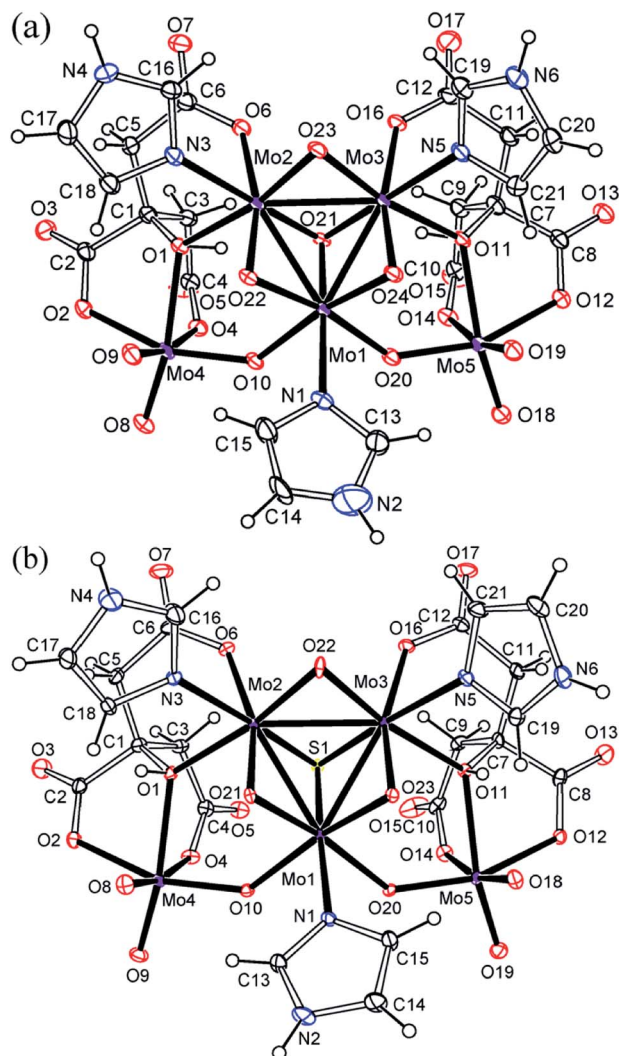


Fig. 1 ORTEP plots of the anion structures in  $K_2(Mo_3^{IV}O_4(im)_3)[Mo^{VI}O_3(Hcit)]_2 \cdot 3im \cdot 4H_2O$  (1, a) and  $(Him)_2(Mo_3^{IV}SO_3(im)_3)[Mo^{VI}O_3-(Hcit)]_2 \cdot im \cdot 6H_2O$  (2, b) at the 20% probability levels.

coordination in 3 is similar to those in FeMo-cofactors of nitrogenases.<sup>5–7</sup> Water molecules act as proton sources around the  $\alpha$ -alkoxy and carboxy groups of homocitrate. It should be highlighted that one water molecule acts as a hydrogen donor for the  $\alpha$ -alkoxy group among the crystallized water molecules, which shows strong hydrogen bonding between the water molecule and the  $\alpha$ -alkoxy group.

As shown by X-ray structural analyses (Fig. 3 and S10<sup>†</sup>),  $(Et_4N)[Mo^{VI}O_2Cl(H_2cit)] \cdot H_2O$  (4) is a monomeric oxomolybdenum(vi) complex. 4 is a product that is captured by a large cation  $(Et_4N)^+$ , while binuclear or tetranuclear molybdenum citrato complexes were usually isolated in acidic conditions in a 1 : 1 ratio.<sup>57,66,67</sup> The molybdenum atom is hexa-coordinated in an approximate octahedral geometry. The citrate ligand uses its  $\alpha$ -alkoxy,  $\alpha$ -carboxy and one  $\beta$ -carboxy acidic groups as a tridentate ligand, while the other  $\beta$ -carboxy acidic group is free. Unlike the coordinated  $\alpha$ -hydroxy groups of citrates in 1 and 2, no protonation was observed for the  $\alpha$ -alkoxy group even under strongly acidic conditions (pH = 0.5). The tridentate

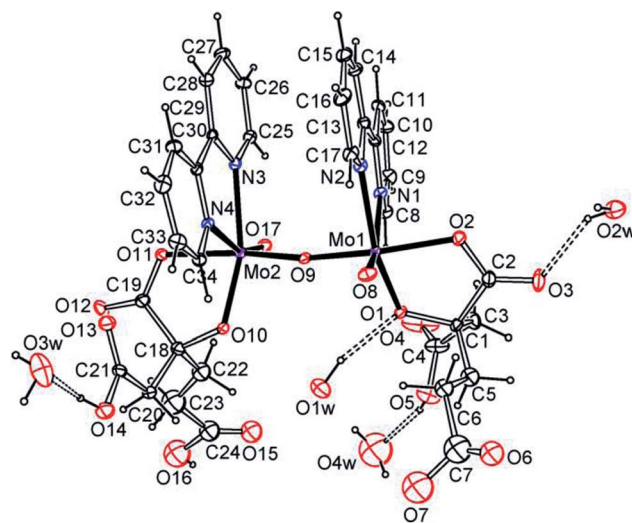


Fig. 2 ORTEP plot of the molecular structure of  $trans-[(Mo^{VO})_2O(H_2-homocit)_2(bpy)_2] \cdot 4H_2O$  (3) at the 20% probability levels.  $[O1 \cdots O1w$  2.74(2),  $O3 \cdots O2w$  2.74(2),  $O14 \cdots O3w$  2.65(2),  $O5 \cdots O4w$  2.60(4) Å].

coordination mode of citrate in 4 is similar to those of  $K_4-[Mo^{VI}O_3(cit)] \cdot 2H_2O$  (6) and  $(NH_4)_4[Mo^{VI}O_3(cit)] \cdot 2H_2O$  (7),<sup>58,66</sup> while both  $\beta$ -carboxy groups of citrate are protonated.

Water cluster and hydrogen bonds also play important roles in the stabilization of the host structures. A crystallized water molecule and a carboxy oxygen atom alternately connect to each other to form a water chain, and two water chains connect to form a band by hydrogen bonds in 4 as shown in Fig. S11.<sup>†</sup> The average  $O \cdots O$  distance of water layer is 2.825 Å shown in Table S3.<sup>†</sup> This is longer than the corresponding value in ice  $I_h$  (2.759 Å)<sup>68</sup> and shorter than in liquid water (2.854 Å),<sup>69,70</sup> but within the values in the ice II phase (2.77–2.84 Å).<sup>71</sup>

Previously, the mimic complexes  $[Mo_3^{IV}SO_3(glyc)_2(im)_5] \cdot im \cdot H_2O$  (13) and  $Na_2[Mo_3^{IV}SO_3(R,S-lact)_3(im)_3] \cdot 10H_2O$  (14) in Table 1 have been used for comparison with FeMo-cofactors in nitrogenases, which provide indirect evidence for the protonation of homocitrate in the FeMo-cofactor  $Mo^{III/IV}Fe_7S_9C(S-cys)(N-His)(homocit)$ .<sup>72</sup> Here the longer  $Mo^{IV}-O$  distances in 1 and 2 [ $2.192(4)_{av}$  Å in 1 and  $2.201(4)_{av}$  Å in 2] further support this

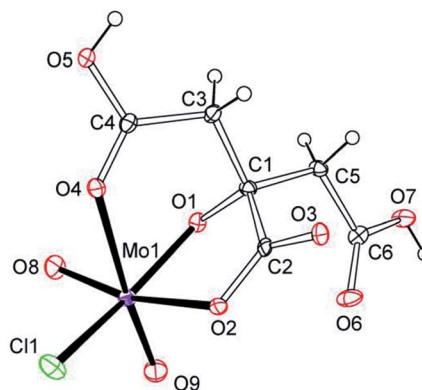


Fig. 3 ORTEP plot of the anion structure in  $(Et_4N)[Mo^{VI}O_2Cl(H_2cit)] \cdot H_2O$  (4) at the 20% probability levels.

proposal that the oxygen atoms in the  $\text{Mo}^{\text{III/IV}}\text{-O}$  ( $\alpha$ -alkoxy/hydroxy) of  $\text{FeMo-co}$  (**16** and **17**) should be protonated,<sup>20–25,73</sup> which are obviously longer than the  $\text{Mo}^{\text{VI}}\text{-O}$  ( $\alpha$ -alkoxy) distances [ $1.975(7)_{\text{av}}$  Å] in **3–14** and similar to the  $\text{Mo}^{\text{IV}}\text{-O}$  ( $\alpha$ -hydroxy) distances [ $2.204(4)_{\text{av}}$  Å] in **15**. The oxygen atom coordinated with molybdenum(IV/VI) was protonated, while the  $\alpha$ -alkoxy group coordinated with molybdenum(VI) in **3** and **4** was deprotonated even under extreme acidic condition. This indicates that the O ( $\alpha$ -alkoxy) coordinated with  $\text{Mo}^{\text{III/IV}}$  atom had a higher charge density and was more easily protonated. The  $\text{Mo}^{\text{IV/VI}}\text{-O}$  ( $\alpha$ -carboxy) and  $\text{Mo}^{\text{VI}}\text{-O}$  ( $\beta$ -carboxy) distances in **1** and **2** were shorter than those of **4** and **6–14**. The characteristic  $\text{Mo}^{\text{IV}}\text{-O-Mo}^{\text{VI}}$  bridges were in apparent asymmetric configurations [ $1.831(4)_{\text{av}}$  and  $2.039(4)_{\text{av}}$  Å]. The Mo–N, Mo– $\mu_2$ -O, Mo– $\mu_3$ -O, Mo–Mo distances in **1**, **2**, **3**, **5**, **13–15** and **18–34** have also been listed for comparison in Table S4.<sup>†</sup><sup>42,43,47,59,72,74–81</sup>

### Solution $^{13}\text{C}$ and $^1\text{H}$ NMR spectra

Solution  $^{13}\text{C}$  and  $^1\text{H}$  NMR spectra are shown in Fig. 4, S12–S21 and Table S5,<sup>†</sup> and provide valuable information on the coordination environments of **1**, **2** and **4**. Only one set of species was observed for **1** and **2** respectively, showing no decomposition over three months. The coordinated  $\alpha$ -carboxy and  $\beta$ -carboxy carbons in **1** and **2** are at around 185.5–185.2 ppm and 181.7–180.5 ppm respectively. Large downfield shifts ( $\Delta_{\alpha\text{-carboxy}} = 5.9\text{--}6.2$  ppm;  $\Delta_{\beta\text{-carboxy}} = 4.5\text{--}5.7$  ppm) are observed compared to those of the free citrate ( $\alpha$ -carboxy 179.3 ppm;  $\beta$ -carboxy 176.0

ppm). The coordinated  $\alpha$ -hydroxy (83.5 ppm in **1** and 82.9 ppm in **2**) and  $\alpha$ -alkoxy carbons (87.0 ppm in **4**) also show large downfield shifts compared to those of the free citrate (75.9 ppm), respectively. The  $^{13}\text{C}$  NMR spectral signals for protonated  $\alpha$ -hydroxy groups in **1** and **2** show an obvious shift to the highfield compared with the  $\alpha$ -alkoxy in **4** and other molybdenum citrates, showing the influence of protonation. The  $\alpha$ -carboxy and methylene carbons in **4**(VI) show downfield shifts compared to those in **1**(IV/VI) and **2**(IV/VI).

### Mo XPS spectra and bond valence calculations

As shown in Table 2, the theoretical bond valence calculations for **1–3** show  $4.274_{\text{av}}$  and  $5.984_{\text{av}}$  for the molybdenum atoms in **2**, respectively, which are close to charge balances +4 and +6. The Mo  $3d_{5/2}$ –Mo  $3d_{3/2}$  doublet was registered at binding energies (BE) 227.3 eV, 230.3 eV and 232.5 eV in the XPS spectrum of **2** as shown in Fig. 5 and S22.<sup>†</sup> The XPS spectrum of bulk  $\text{MoO}_3$  in the Mo 3d region showed a single spin–orbit doublet with a Mo  $3d_{5/2}$  binding energy of 233.0 eV.<sup>84,85</sup> The widening of the Mo 3d level is associated with the presence of more than one molybdenum states.<sup>86–89</sup> The Mo  $3d_{5/2}$  peak at BE = 232.5 eV is characteristic of the  $\text{Mo}^{\text{VI}}$  presence, while Mo  $3d_{5/2}$  and Mo  $3d_{3/2}$  peaks at BE = 230.3 eV and 227.3 eV are attributed to the  $\text{Mo}^{\text{IV}}$  species.

### EPR spectrum and magnetic susceptibility

Theoretical bond valence calculations give the valences  $5.232_{\text{av}}$  for molybdenum atoms in **3**, which is close to a charge balance

**Table 1** Comparison of selected Mo–O bond distances (Å) for  $\text{K}_2(\text{Mo}_3^{\text{IV}}\text{O}_4(\text{im})_3[\text{Mo}^{\text{VI}}\text{O}_3(\text{Hcit})]_2) \cdot 3\text{im} \cdot 4\text{H}_2\text{O}$  (**1**),  $(\text{Him})_2(\text{Mo}_3^{\text{IV}}\text{SO}_3(\text{im})_3[\text{Mo}^{\text{VI}}\text{O}_3(\text{Hcit})]_2) \cdot \text{im} \cdot 6\text{H}_2\text{O}$  (**2**), *trans*- $[(\text{Mo}^{\text{VO}}\text{O}_2(\text{H}_2\text{homocit})_2(\text{bpy})_2) \cdot 4\text{H}_2\text{O}$  (**3**),  $(\text{Et}_4\text{N})[\text{Mo}^{\text{VI}}\text{O}_2\text{Cl}(\text{H}_2\text{cit})] \cdot \text{H}_2\text{O}$  (**4**),  $(\text{Mo}^{\text{VO}}\text{O}_2\text{O}(\text{H}_2\text{cit})_2(\text{bpy})_2) \cdot 4\text{H}_2\text{O}$  (**5**),<sup>81</sup>  $\text{K}_4[\text{Mo}^{\text{VI}}\text{O}_3(\text{cit})] \cdot 2\text{H}_2\text{O}$  (**6**),<sup>66</sup>  $(\text{NH}_4)_4[\text{Mo}^{\text{VI}}\text{O}_3(\text{cit})] \cdot 2\text{H}_2\text{O}$  (**7**),<sup>58</sup>  $\text{Na}_2[\text{Mo}^{\text{VI}}\text{O}_2(\text{H}_2\text{cit})_2] \cdot 3\text{H}_2\text{O}$  (**8**),<sup>56</sup>  $\text{K}_2[(\text{Mo}^{\text{VI}}\text{O}_2)_2\text{O}(\text{H}_2\text{cit})_2] \cdot 4\text{H}_2\text{O}$  (**9**),<sup>58</sup>  $\text{K}_2[\text{Mo}^{\text{VI}}\text{O}_2(\text{H}_2\text{homocit})_2] \cdot 2\text{H}_2\text{O}$  (**10**),<sup>65</sup>  $\text{K}_2(\text{NH}_4)_2[(\text{Mo}^{\text{VI}}\text{O}_2)_4\text{O}_3(\text{Hhomocit})_2] \cdot 6\text{H}_2\text{O}$  (**11**),<sup>64</sup>  $\text{K}_5[(\text{Mo}^{\text{VI}}\text{O}_2)_4\text{O}_3(\text{Hhomocit})_2]\text{Cl} \cdot 5\text{H}_2\text{O}$  (**12**),<sup>64</sup>  $[\text{Mo}_3^{\text{IV}}\text{SO}_3(\text{glyc})(\text{im})_5] \cdot \text{im} \cdot \text{H}_2\text{O}$  (**13**),<sup>72</sup>  $\text{Na}_2[\text{Mo}_3^{\text{IV}}\text{SO}_3(\text{R,S-lact})_3(\text{im})_3] \cdot 10\text{H}_2\text{O}$  (**14**),<sup>72</sup>  $[\text{Mo}_3^{\text{IV}}\text{S}_4(\text{PPh}_3)_3(\text{Hlact})_2(\text{lact})]$  (**15**),<sup>80</sup>  $\text{FeMo-cofactors } \{\text{Mo}^{\text{III/IV}}\text{Fe}_7\text{S}_9\text{C}(\text{S-cys})(\text{N-His})(\text{Hhomocit})\}$  (**16**) (**a**, PDB 1QGU;<sup>82</sup> **b**, PDB 1M1N;<sup>8</sup> **c**, PDB 3K1A;<sup>83</sup> **d**, PDB 3U7Q<sup>9</sup>) and  $\text{MoFe}_7\text{S}_9\text{C}(\text{S-cys})(\text{N-His})(\text{Hcit})$  (**17**) (PDB 1H1L<sup>32</sup>)

Complexes ( $\text{Mo}^{n+}$ )	Mo–O $_{\alpha\text{-alkoxy/hydroxy}}$	Mo–O $_{\alpha\text{-carboxy}}$	Mo–O $_{\beta\text{-carboxy}}$
<b>1</b> (IV/VI)	2.151(4) <sub>av</sub> (IV) 2.192(4) <sub>av</sub> (VI)	2.101(5) <sub>av</sub>	2.071(5) <sub>av</sub> (IV) 2.259(5) <sub>av</sub> (VI)
<b>2</b> (IV/VI)	2.189(4) <sub>av</sub> (IV) 2.201(4) <sub>av</sub> (VI)	2.104(4) <sub>av</sub>	2.079(4) <sub>av</sub> (IV) 2.269(4) <sub>av</sub> (VI)
<b>5</b> (V) <sup>81</sup>	1.982(3) <sub>av</sub>	2.076(3) <sub>av</sub>	
<b>3</b> (V)	1.952(1) <sub>av</sub>	2.068(2) <sub>av</sub>	
<b>4</b> (VI)	1.931(4)	2.178(3)	2.433(4)
<b>6</b> (VI) <sup>66</sup>	2.052(2)	2.237(7)	2.411(3)
<b>7</b> (VI) <sup>58</sup>	2.054(1)	2.213(1)	2.307(2)
<b>8</b> (VI) <sup>56</sup>	1.957(7) <sub>av</sub>	2.219(7) <sub>av</sub>	
<b>9</b> (VI) <sup>58</sup>	1.919(2)	2.178(3)	2.538(2)
<b>10</b> (VI) <sup>65</sup>	1.984(1) <sub>av</sub>	2.209(1) <sub>av</sub>	
<b>11</b> (VI) <sup>64</sup>	1.942(4) <sub>av</sub>	2.188(4) <sub>av</sub>	2.322(4) <sub>av</sub>
<b>12</b> (VI) <sup>64</sup>	1.939(3) <sub>av</sub>	2.197(3) <sub>av</sub>	2.304(3) <sub>av</sub>
<b>13</b> (IV) <sup>72</sup>	1.986(2) <sub>av</sub>	2.127(2) <sub>av</sub>	
<b>14</b> (IV) <sup>72</sup>	1.999(7) <sub>av</sub>	2.133(6) <sub>av</sub>	
<b>15</b> (IV) <sup>80</sup>	2.092(3)/2.204(4) <sub>av</sub>	2.083(4)/2.118(4) <sub>av</sub>	
<b>16a</b> <sup>82</sup>	2.351	2.293	
<b>16b</b> <sup>8</sup>	2.199	2.181	
<b>16c</b> <sup>83</sup>	2.250	2.171	
<b>16d</b> <sup>9</sup>	2.178	2.212	
<b>17</b> <sup>32</sup>	2.252	2.292	



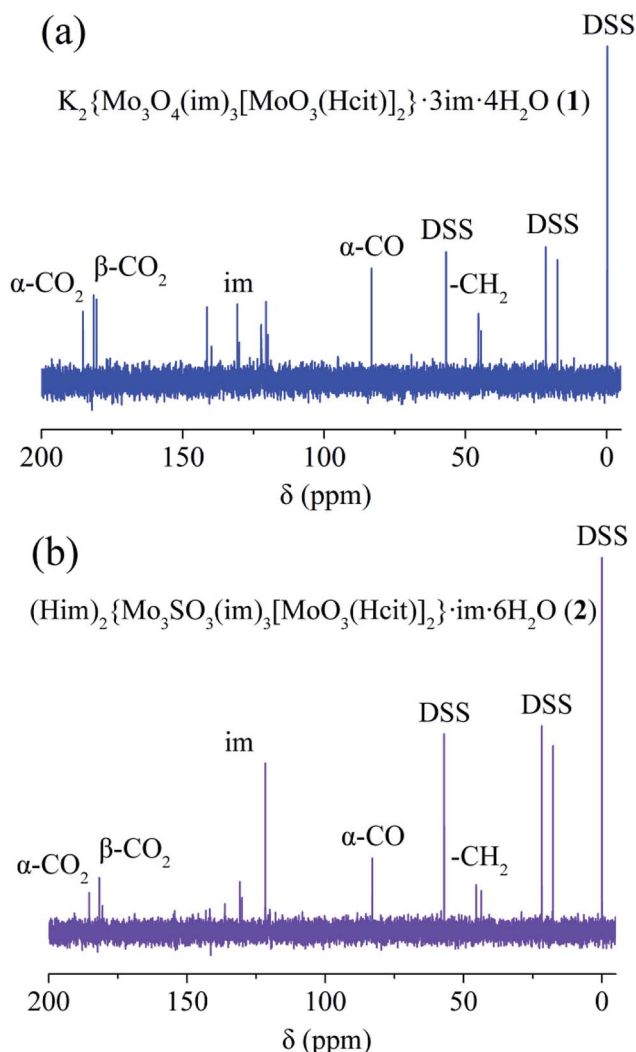


Fig. 4  $^{13}\text{C}$  NMR spectra of  $\text{K}_2\{\text{Mo}_3\text{O}_4(\text{im})_3[\text{Mo}^{\text{VI}}\text{O}_3(\text{Hcit})_2]\} \cdot 3\text{im} \cdot 4\text{H}_2\text{O}$  (1, a),  $(\text{Him})_2\{\text{Mo}_3\text{SO}_3(\text{im})_3[\text{Mo}^{\text{VI}}\text{O}_3(\text{Hcit})_2]\} \cdot \text{im} \cdot 6\text{H}_2\text{O}$  (2, b).

of +5. The two molybdenum atoms in 3 are independently paramagnetic, based on the X-band of solid state EPR spectrum at 90 K as shown in Fig. 6.<sup>90,91</sup> The EPR spectrum of 3 appeared to be anisotropic, and the  $g$  value was 1.9089. The bands which exhibit  $S = 1/2$  signals are consistent with a  $4d^1$  metal center  $\text{Mo}^{5+}$ , while neither  $\text{Mo}^{4+}$  or  $\text{Mo}^{6+}$  in 2 had an EPR signal. 2 and 3 with valences of  $\text{Mo}(\text{IV}/\text{VI})$  or  $\text{Mo}(\text{V})$  atoms exhibit diamagnetism as shown in Fig. S23 and S24† respectively.<sup>92–94</sup>

### IR and UV-visible spectra

1–4 were also characterized by IR and UV-Vis spectroscopies respectively. Based on the IR spectra shown in Fig. S25–S27,† vibrations of the symmetric and asymmetric carboxy groups,  $\text{Mo}=\text{O}$  and  $\text{Mo}-\text{O}-\text{Mo}$  bonds appeared at  $1683\text{--}1612\text{ cm}^{-1}$ ,  $1427\text{--}1364\text{ cm}^{-1}$ ,  $949\text{--}850\text{ cm}^{-1}$  and  $722\text{--}704\text{ cm}^{-1}$ , respectively. The absorptions of carboxy acidic groups for 3 and 4 appeared at  $1724\text{ cm}^{-1}$  and  $1732\text{ cm}^{-1}$ . Due to the chelation of the five-membered rings with molybdenum atoms, the symmetric and asymmetric absorption peaks of the carboxy

Table 2 Bond valence calculations for  $\text{K}_2\{\text{Mo}_3^{\text{IV}}\text{O}_4(\text{im})_3[\text{Mo}^{\text{VI}}\text{O}_3(\text{Hcit})_2]\} \cdot 3\text{im} \cdot 4\text{H}_2\text{O}$  (1),  $(\text{Him})_2\{\text{Mo}_3^{\text{IV}}\text{SO}_3(\text{im})_3[\text{Mo}^{\text{VI}}\text{O}_3(\text{Hcit})_2]\} \cdot \text{im} \cdot 6\text{H}_2\text{O}$  (2),  $\text{trans}-[(\text{Mo}^{\text{VO}})_2\text{O}(\text{H}_2\text{homocit})_2(\text{bpy})_2] \cdot 4\text{H}_2\text{O}$  (3) and  $(\text{Et}_4\text{N})[\text{Mo}^{\text{VI}}\text{O}_2\text{Cl}(\text{H}_2\text{cit})] \cdot \text{H}_2\text{O}$  (4)

Complexes	Atom	N	$\sum S_{ij}$	$\Delta$
1	Mo(1)	4+	4.341	0.341
	Mo(2)	4+	4.263	0.263
	Mo(3)	4+	4.283	0.283
	Mo(4)	6+	5.993	0.007
	Mo(5)	6+	5.970	0.030
2	Mo(1)	4+	4.439	0.439
	Mo(2)	4+	4.207	0.207
	Mo(3)	4+	4.177	0.177
	Mo(4)	6+	5.944	0.056
	Mo(5)	6+	6.023	0.023
3	Mo(1)	5+	5.208	0.208
	Mo(2)	5+	5.256	0.256
4	Mo(1)	6+	6.012	0.012

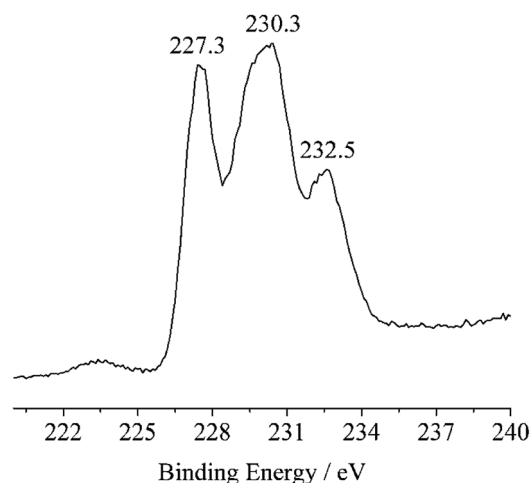


Fig. 5 XPS spectrum (Mo 3d level) of  $(\text{Him})_2\{\text{Mo}_3^{\text{IV}}\text{SO}_3(\text{im})_3[\text{Mo}^{\text{VI}}\text{O}_3(\text{Hcit})_2]\} \cdot \text{im} \cdot 6\text{H}_2\text{O}$  (2).

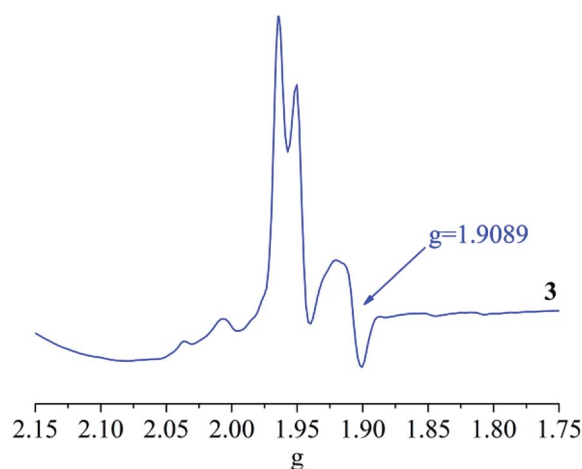


Fig. 6 EPR spectrum of  $\text{trans}-[(\text{Mo}^{\text{VO}})_2\text{O}(\text{H}_2\text{homocit})_2(\text{bpy})_2] \cdot 4\text{H}_2\text{O}$  (3).



groups were red shifted to low wave numbers. In the UV-Vis spectra, the strong absorption peaks were due to ligand-based  $\pi-\pi^*$  transitions (206 nm in **1** and 207 nm in **2**) and intra ligand transitions (230 nm in **1** and 231 nm in **2**) as shown in Fig. S28.† The strong absorption peaks of bipyridine appeared at 280 nm in **3** due to the N-chelating ligand-based  $\pi-\pi^*$  transition as shown in Fig. S29.†

### Cyclic voltammograms and mass spectra

Cyclic voltammograms of **1**, **2** and **4** scanning from  $-1.600$  V to  $1.600$  V were performed in  $1 \text{ mol L}^{-1} \text{ Na}_2\text{SO}_4$  aqueous solution as shown in Fig. S30–S32.† The CV scan measurements were made in the positive direction, and then back to the cathode reduction region. As for the cyclic voltammograms of **1** and **2**, the reductive waves of  $\text{Mo}^{\text{VI}}$  appeared at  $-0.567$  V and  $-0.564$  V, respectively. The oxidized peak of  $\text{Mo}^{\text{IV}}$  in **1** was at  $+0.776$  V, while there was no oxidized peak in **2**. **2** with a central sulfur atom is more easily reduced than **1** with its central oxygen atom. The fact indicates that  $\text{Mo}^{\text{IV}}$  atoms in  $[\text{Mo}_3^{\text{IV}}\text{SO}_3]^{4+}$  were more stable than those in  $[\text{Mo}_3^{\text{IV}}\text{O}_4]^{4+}$  and not easily oxidized. All redox

processes were single and irreversible, which are different from those previously reported for  $[\text{Mo}_3^{\text{IV}}\text{O}_4(\text{ox})_3]^{2-}$ .<sup>47,95</sup> Mass spectra of major anions in **1**, **2** and **3** are shown in Fig. 7 and S33.† As the ion source bombarded the complexes, the imidazoles and chlorides that are weakly coordinated with the metal dissociated, and there were no peaks associated with the complete anions in the spectra, except for  $\{\text{Mo}_3^{\text{IV}}\text{O}_4[\text{Mo}^{\text{VI}}\text{O}_3(\text{Hcit})]_2\}^{2-}$  ( $\{\text{Mo}_3^{\text{IV}}\text{SO}_3[\text{Mo}^{\text{VI}}\text{O}_3(\text{Hcit})]_2\}^{2-}$ ) and  $[\text{Mo}^{\text{VI}}\text{O}_2(\text{Hcit})]^{1-}$ .

## Conclusions

A series of molybdenum(IV/V/VI) citrates and homocitrate  $\text{K}_2$ - $\{\text{Mo}_3^{\text{IV}}\text{O}_4(\text{im})_3[\text{Mo}^{\text{VI}}\text{O}_3(\text{Hcit})]_2\} \cdot 3\text{im} \cdot 4\text{H}_2\text{O}$  (**1**),  $(\text{Him})_2\{\text{Mo}_3^{\text{IV}}\text{SO}_3(\text{im})_3[\text{Mo}^{\text{VI}}\text{O}_3(\text{Hcit})]_2\} \cdot \text{im} \cdot 6\text{H}_2\text{O}$  (**2**), *trans*- $[(\text{Mo}^{\text{VO}})_2\text{O}(\text{H}_2\text{homocit})_2(\text{bpy})_2] \cdot 4\text{H}_2\text{O}$  (**3**) and  $(\text{Et}_4\text{N})[\text{Mo}^{\text{VI}}\text{O}_2\text{Cl}(\text{H}_2\text{cit})] \cdot \text{H}_2\text{O}$  (**4**) were prepared from aqueous solutions. Pentanuclear imidazole hydrocitrato molybdenum(IV/VI) complexes **1** and **2** were obtained with incomplete cubane units  $[\text{Mo}_3^{\text{IV}}\text{SO}_3]^{4+}$  and  $[\text{Mo}_3^{\text{IV}}\text{O}_4]^{4+}$  units. The charge balances, theoretical bond valence calculations and XPS spectrum indicate molybdenum atoms with valences of +4 or +6 respectively, which are different from the mixed-valence complexes in the adjacent valence state. The incomplete cubane cluster units,  $[\text{Mo}_3^{\text{IV}}\text{SO}_3]^{4+}$  and  $[\text{Mo}_3^{\text{IV}}\text{O}_4]^{4+}$ , with monodentate imidazoles were coordinated by two  $[\text{Mo}^{\text{VI}}\text{O}_3(\text{Hcit})]^{3-}$  anions on both sides to form pentanuclear skeleton structures. It is worth noting that the  $\alpha$ -alkoxy groups of coordinated citrates in **1** and **2** were protonated, indicating O ( $\alpha$ -hydroxy) atoms in molybdenum(IV) complexes with higher charge densities are more easily protonated. The structures in **1** and **2** are important for the further study of imidazole molybdenum complexes with  $\alpha$ -hydroxycarboxylates. The homocitrate anions in **3** chelate to Mo *via* the  $\alpha$ -alkoxy and monodentate  $\alpha$ -carboxy groups, while the remaining  $\beta$ - and  $\gamma$ -carboxylic acid groups remained free. Moreover, the monomeric oxomolybdenum citrate complex  $(\text{Et}_4\text{N})[\text{Mo}^{\text{VI}}\text{O}_2\text{Cl}(\text{H}_2\text{cit})] \cdot \text{H}_2\text{O}$  (**4**) is captured by large cations  $[\text{Et}_4\text{N}]^+$  with  $\alpha$ -alkoxy coordination in strong acidic conditions. The solution behaviors of **1** and **2** were discussed based on  $^1\text{H}$  and  $^{13}\text{C}$  NMR spectroscopies giving only one set of species, and showing no decomposition of **1** and **2**. The coordinated  $\alpha$ -alkoxy/hydroxyl and carboxy carbons in **1**, **2** and **4** show large downfield shifts compared with those of the free citrate. The cyclic voltammograms of **1** and **2** indicate that  $\text{Mo}^{\text{IV}}$  atoms in  $[\text{Mo}_3^{\text{IV}}\text{SO}_3]^{4+}$  were more stable than that in  $[\text{Mo}_3^{\text{IV}}\text{O}_4]^{4+}$ . **2** and **3** exhibited diamagnetically.

## Experimental

**Preparations of  $\text{K}_2\{\text{Mo}_3^{\text{IV}}\text{O}_4(\text{im})_3[\text{Mo}^{\text{VI}}\text{O}_3(\text{Hcit})]_2\} \cdot 3\text{im} \cdot 4\text{H}_2\text{O}$  (**1**) and  $(\text{Him})_2\{\text{Mo}_3^{\text{IV}}\text{SO}_3(\text{im})_3[\text{Mo}^{\text{VI}}\text{O}_3(\text{Hcit})]_2\} \cdot \text{im} \cdot 6\text{H}_2\text{O}$  (**2**)**

$(\text{NH}_4)_6\text{Mo}_7\text{O}_{24} \cdot 4\text{H}_2\text{O}$  (0.35 g, 0.29 mmol), citric acid (0.42 g, 2.0 mmol), imidazole (0.136 g, 2.0 mmol) were dissolved in 10 mL water, then excess hydrazine dihydrochloride (0.42 g, 4.0 mmol) was added in an anaerobic environment. The pH value was adjusted to 9.5 by the addition of KOH solution (5.0 M). The reactants were heated at  $120^\circ\text{C}$  for 24 h in a 10 mL Teflon-lined

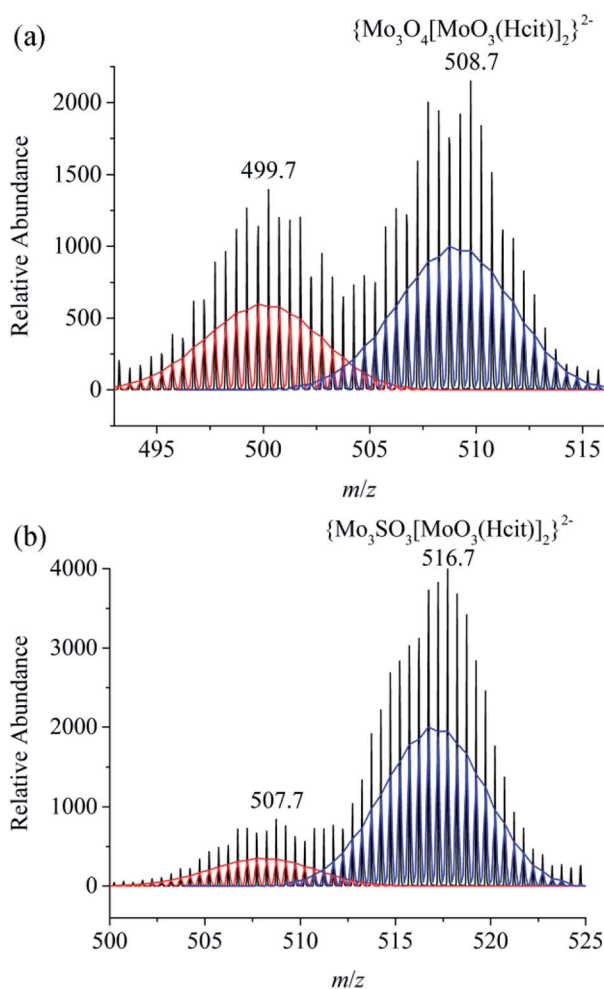


Fig. 7 Mass spectra of  $\{\text{Mo}_3\text{O}_4[\text{Mo}^{\text{VI}}\text{O}_3(\text{Hcit})]_2\}^{2-}$  and  $\{\text{Mo}_3\text{SO}_3[\text{Mo}^{\text{VI}}\text{O}_3(\text{Hcit})]_2\}^{2-}$  in  $\text{K}_2\{\text{Mo}_3^{\text{IV}}\text{O}_4(\text{im})_3[\text{Mo}^{\text{VI}}\text{O}_3(\text{Hcit})]_2\} \cdot 3\text{im} \cdot 4\text{H}_2\text{O}$  (**1**, a) and  $(\text{Him})_2\{\text{Mo}_3^{\text{IV}}\text{SO}_3(\text{im})_3[\text{Mo}^{\text{VI}}\text{O}_3(\text{Hcit})]_2\} \cdot \text{im} \cdot 6\text{H}_2\text{O}$  (**2**, b) respectively.



stainless steel container under aqueous reaction conditions and cooled to room temperature. Product **1** was isolated as yellow needle crystals after one month in 6.7% yields (0.042 g) based on molybdenum. Found (calcd for  $C_{30}H_{42}N_{12}O_{28}Mo_5K_2$ ): C, 22.7 (22.9); H, 3.0 (2.7); N, 10.4 (10.7). IR (KBr,  $cm^{-1}$ ):  $\nu(C-H)$  3124<sub>w</sub>, 2954<sub>w</sub>, 2852<sub>w</sub>;  $\nu_{as}(CO_2)$  1640<sub>vs</sub>;  $\nu_s(CO_2)$  1397<sub>s</sub>;  $\nu_s(Mo=O)$  916<sub>s</sub>;  $\nu_{as}(Mo-O-Mo)$  704<sub>s</sub>. UV-Vis ( $H_2O$ , nm): 206, 230. Solution  $^1H$  NMR (400 MHz,  $D_2O$ , 25 °C, DSS):  $\delta$  = 8.64 (s, 2H; CH), 8.48 (s, 1H; CH), 8.31 (s, 2H; CH), 7.73 (s, 3H; CH), 7.31 (t,  $J$  = 3 Hz, 3H; CH), 7.26 (d,  $J$  = 2 Hz, 7H; CH), 2.91 (t,  $J$  = 8 Hz, 8H;  $CH_2$ ); solution  $^{13}C$  NMR (100 MHz,  $D_2O$ , 25 °C, DSS):  $\delta$  = 185.2 ppm, 181.5 ppm, 180.5 ppm, 141.4 ppm, 130.7 ppm, 120.6 ppm, 83.3 ppm, 45.4 ppm, 44.5 ppm.

Similarly, the synthesis of **2** was performed, except  $Na_2S_2O_4$  (0.35 g, 2.0 mmol) was used instead of hydrazine dihydrochloride and the pH value was adjusted to 6.0 with the addition of NaOH solution (5.0 M). Product **2** was isolated as green plates after one month in 10.5% yields (0.065 g) based on molybdenum. Found (calcd for  $C_{30}H_{48}N_{12}O_{29}SMo_5$ ): C, 22.9 (23.2); H, 3.3 (3.1); N, 10.7 (10.8). IR (KBr,  $cm^{-1}$ ):  $\nu(C-H)$  3128<sub>w</sub>, 2957<sub>w</sub>, 2853<sub>w</sub>;  $\nu_{as}(CO_2)$  1626<sub>vs</sub>;  $\nu_s(CO_2)$  1399<sub>s</sub>;  $\nu_s(Mo=O)$  921<sub>s</sub>;  $\nu_{as}(Mo-O-Mo)$  712<sub>s</sub>. UV-Vis ( $H_2O$ , nm): 207, 231. Solution  $^1H$  NMR (400 MHz,  $D_2O$ , 25 °C, DSS):  $\delta$  = 8.69 (d,  $J$  = 10 Hz, 4H; CH), 8.61 (s, 1H; CH), 7.86 (s, 1H; CH), 7.77 (s, 2H; CH), 7.45 (s, 7H; CH), 7.35 (s, 2H; CH), 7.30 (s, 1H; CH), 2.81 (t,  $J$  = 8 Hz, 8H;  $CH_2$ ); solution  $^{13}C$  NMR (100 MHz,  $D_2O$ , 25 °C, DSS):  $\delta$  = 185.4 ppm, 181.7 ppm, 130.8 ppm, 121.7 ppm, 82.9 ppm, 45.5 ppm, 43.6 ppm.

### Preparation of *trans*-( $Mo^V O_2 O(H_2 homocit)_2(bpy)_2$ )·4H<sub>2</sub>O (**3**)

The homocitric acid  $\gamma$ -lactone (0.060 g, 0.30 mmol)<sup>96</sup> synthesized by five steps was dissolved in a minimal amount of water. The pH was adjusted to 11 by the addition of potassium hydroxide to generate the acyclic homocitrate. The mixture was stirred for two days to complete the hydrolysis at room temperature.  $(NH_4)_6Mo_7O_{24} \cdot 4H_2O$  (0.026 g, 0.021 mmol) and 1.0 mL 2,2'-bipyridine ethanol solution (0.15 mol  $mL^{-1}$ ) was added and the solution was stirred for one hour, then excess hydrazine dihydrochloride (0.060 g, 0.60 mmol) was added. The pH value was adjusted to 2.5 with the addition of hydrochloric acid. A dark purple solution was obtained when 1.0 mL 2,2'-bipyridine ethanol solution (0.30 mmol  $mL^{-1}$ ) was added. Product **3** was isolated as purple plates in 20.7% yields (0.016 g) based on molybdenum after one day. Found (calcd for  $C_{34}H_{40}N_4O_{21}Mo_2$ ): C, 39.3 (39.6); H, 4.0 (3.9); N, 5.3 (5.4). IR (KBr,  $cm^{-1}$ ):  $\nu(\beta-CO_2H)$  1724<sub>vs</sub>;  $\nu_{as}(CO_2)$  1639<sub>vs</sub>;  $\nu_s(CO_2)$  1427<sub>s</sub>, 1402<sub>s</sub>;  $\nu_s(Mo=O)$  947<sub>m</sub>, 871<sub>w</sub>, 850<sub>m</sub>;  $\nu_{as}(Mo-O-Mo)$  722<sub>m</sub>. UV (DMSO, nm): 280, 315, 422, 593.

### Preparation of $(Et_4N)[Mo^VI O_2 Cl(H_2 cit)] \cdot H_2O$ (**4**)

$(NH_4)_4[Mo^VI O_3(cit)] \cdot 2H_2O$ <sup>98</sup> (0.44 g, 1.0 mmol) and tetraethylammonium chloride (0.17 g, 1.0 mmol) were mixed in 10 mL water. The pH value was adjusted to 0.5 with dilute hydrochloric acid. The resulting solution was allowed to stand at room temperature and slow evaporation afforded colorless crystals of **4** with 52.5% yield (0.026 g) based on molybdenum.

Found (calcd for  $C_{14}H_{28}NO_{10}ClMo$ ): C, 33.4 (33.5); H, 5.4 (5.6); N, 2.5 (2.8). IR (KBr,  $cm^{-1}$ ):  $\nu(\beta-CO_2H)$  1732<sub>vs</sub>;  $\nu_{as}(CO_2)$  1683<sub>vs</sub>, 1612<sub>vs</sub>;  $\nu_s(CO_2)$  1364<sub>vs</sub>;  $\nu_s(Mo=O)$  949<sub>vs</sub>, 909<sub>vs</sub>, 850<sub>s</sub>. Solution  $^1H$  NMR (400 MHz,  $D_2O$ , 25 °C, DSS):  $\delta$  = 3.25 ( $q_{AB}$ ,  $J$  = 7 Hz, 8H;  $CH_2-N$ ), 3.03–2.86 (d–d,  $J$  = 16 Hz, 4H;  $CH_2$ ), 1.28–1.24 (m,  $J$  = 2 Hz, 12H;  $CH_3$ ); solution  $^{13}C$  NMR (100 MHz,  $D_2O$ , 25 °C, DSS):  $\delta$  = 185.8 ppm, 175.8 ppm, 87.0 ppm, 54.5 ppm, 45.6 ppm, 9.2 ppm.

### X-ray structure determinations

Crystals **1–4** were measured on an Oxford Gemini CCD diffractometer with graphite monochromatic  $Mo-K\alpha$  radiation ( $\lambda$  = 0.71073 Å) or  $Cu-K\alpha$  radiation ( $\lambda$  = 1.54184 Å) at 173 K. The structures were primarily solved by Olex2 and ShelXT in WinGX program<sup>97</sup> and refined by full-matrix least-squares procedures with anisotropic thermal parameters for all of the nonhydrogen atoms with SHELX-2014/7.<sup>98–100</sup> Crystallographic data and structural refinements for **1–4** are listed in Table S6.† Selected bond distances and angles are listed in Tables S7–S10.†

### Physical measurements

Infrared spectra were recorded as Nujol mulls between KBr plates on a Nicolet 380 FT-IR spectrometer. Elemental analyses were performed with a Vario EL III elemental analyzer. UV-visible spectra were recorded on a Shimadzu UV-Vis 2550 spectrophotometer. Solution  $^1H$  NMR and  $^{13}C$  NMR spectra were recorded on a Bruker AV 500 NMR spectrometer with  $D_2O$  using DSS (sodium 2,2-dimethyl-2-silapentane-5-sulfonate) as an internal reference. The magnetic susceptibility of microcrystalline sample restrained in parafilm was measured on a Quantum Design MPMS.XL-7 magnetometer with an applied field of 5 kOe. Cyclic voltammetry measurements were carried out on a CHI 720E electrochemical station using a conventional three-electrode single compartment cell at room temperature under a nitrogen atmosphere. The working electrode was glassy carbon, a platinum plate was used as the counter electrode and  $Hg/Hg_2Cl_2$  as the reference electrode. Mass spectra were recorded on an Agilent 6224 mass spectrometer. The XPS spectra were recorded on a Qtac-100 LEISS-XPS spectrometer with a hemispherical detector operating at constant pass energy (PE = 40 eV) and pressure  $1 \times 10^{-8}$  Pa. An X-ray source of power 300 W ( $I$  = 20 mA,  $U$  = 15 kV) and Al  $K\alpha$  radiation ( $E_{\gamma} = h\nu = 1486.6$  eV) were used. The sample temperature was 25 °C. All the binding energies (BE) were referenced to the C 1s line at 285 eV. Electron paramagnetic resonance (EPR) was recorded on Bruker EMX-10/12 electron paramagnetic resonance spectrometer. The magnetic susceptibility of microcrystalline samples restrained in parafilm was measured on a Quantum Design MPMS.XL-7 magnetometer with an applied field of 5 kOe.

### Conflicts of interest

There are no conflicts to declare.



## Acknowledgements

We thank the supports from the National Science Foundation (21773196) and the National Science Foundation of Fujian (2016J0101) for their generous financial supports. Thanks to engineers Shen-Shui Yu, Shui-Chao Lin, Hai-Yan Shi, Yan-Ping Zheng, Dr An-Ni Feng and Dr Ying-Zi Han for their helps in spectral measurements.

## Notes and references

- 1 K. Heinze, *Coord. Chem. Rev.*, 2015, **300**, 121–141.
- 2 R. Hille, J. Hall and P. Basu, *Chem. Rev.*, 2014, **114**, 3963–4038.
- 3 T. R. Hoover, A. D. Robertson, R. L. Cerny, R. N. Hayes, J. Imperial, V. K. Shah and P. W. Ludden, *Nature*, 1987, **329**, 855–857.
- 4 T. R. Hoover, J. Imperial, P. W. Ludden and V. K. Shah, *Biochemistry*, 1989, **28**, 2768–2771.
- 5 J. Kim and D. C. Rees, *Nature*, 1992, **360**, 553–560.
- 6 J. Kim and D. C. Rees, *Science*, 1992, **257**, 1677–1682.
- 7 M. M. Georgiadis, H. Komiya, P. Chakrabarti, D. Woo, J. J. Kornuc and D. C. Rees, *Science*, 1992, **257**, 1653–1659.
- 8 O. Einsle, F. A. Tezcan, S. L. A. Andrade, B. Schmid, M. Yoshida, J. B. Howard and D. C. Rees, *Science*, 2002, **297**, 1696–1700.
- 9 T. Spatzal, M. Aksoyoglu, L. Zhang, S. L. A. Andrade, E. Schleicher, S. Weber, D. C. Rees and O. Einsle, *Science*, 2011, **334**, 940.
- 10 K. M. Lancaster, M. Roemelt, P. Ettenhuber, Y. Hu, M. W. Ribbe, F. Neese, U. Bergmann and S. DeBeer, *Science*, 2011, **334**, 974–977.
- 11 B. Schmid, M. W. Ribbe, O. Einsle, M. Yoshida, L. M. Thomas, D. R. Dean, D. C. Rees and B. K. Burgess, *Science*, 2002, **296**, 352–356.
- 12 F. Fazius, E. Shelest, P. Gebhardt and M. Brock, *Mol. Microbiol.*, 2012, **86**, 1508–1530.
- 13 T. M. Zabriskie and M. D. Jackson, *Nat. Prod. Rep.*, 2000, **17**, 85–97.
- 14 H. Quezada, A. Marin Hernandez, D. Aguilar, G. Lopez, J. C. Gallardo Perez, R. Jasso Chavez, A. Gonzalez, E. Saavedra and R. Moreno Sanchez, *Mol. Microbiol.*, 2011, **82**, 578–590.
- 15 Y. Hu, M. C. Corbett, A. W. Fay, J. A. Webber, K. O. Hodgson, B. Hedman and M. W. Ribbe, *Proc. Natl. Acad. Sci. U. S. A.*, 2006, **103**, 17125–17130.
- 16 Y. Hu and M. W. Ribbe, *Microbiol. Mol. Biol. Rev.*, 2011, **75**, 664–677.
- 17 K. L. C. Groenberg, C. A. Gormal, M. C. Durrant, B. E. Smith and R. A. Henderson, *J. Am. Chem. Soc.*, 1998, **120**, 10613–10621.
- 18 M. A. Walters, S. K. Chapman and W. H. Orme Johnson, *Polyhedron*, 1986, **5**, 561–565.
- 19 I. Dance, *Dalton Trans.*, 2008, 5977–5991.
- 20 C. Y. Chen, M. L. Chen, H. B. Chen, H. Wang, S. P. Cramer and Z. H. Zhou, *J. Inorg. Biochem.*, 2014, **141**, 114–120.
- 21 Q. Chen, H. Chen, Z. Cao, Z. Zhou, H. Wan, Y. Li and J. Li, *Sci. Sin.: Chim.*, 2014, **44**, 1849–1864.
- 22 B. M. Hoffman, D. Lukoyanov, Z. Y. Yang, D. R. Dean and L. C. Seefeldt, *Chem. Rev.*, 2014, **114**, 4041–4062.
- 23 B. Benediktsson and R. Bjornsson, *Inorg. Chem.*, 2017, **56**, 13417–13429.
- 24 L. Cao, O. Caldararu and U. Ryde, *J. Phys. Chem. B*, 2017, **121**, 8242–8262.
- 25 C. N. Morrison, T. Spatzal and D. C. Rees, *J. Am. Chem. Soc.*, 2017, **139**, 10856–10862.
- 26 J. Bergwerff, M. Jansen, B. Leliveld, T. Visser, K. Dejong and B. Weckhuysen, *J. Catal.*, 2006, **243**, 292–302.
- 27 O. V. Klimov, A. V. Pashigreva, M. A. Fedotov, D. I. Kochubey, Y. A. Chesalov, G. A. Bukhtiyarova and A. S. Noskov, *J. Mol. Catal. A: Chem.*, 2010, **322**, 80–89.
- 28 M. A. Lélías, P. J. Kooyman, L. Mariey, L. Oliviero, A. Travert, J. van Gestel, J. A. R. van Veen and F. Maugé, *J. Catal.*, 2009, **267**, 14–23.
- 29 Y. Zeng, Z. Li, M. Ma and S. Zhou, *Electrochem. Commun.*, 2000, **2**, 36–38.
- 30 L. S. Sanches, S. H. Domingues, C. E. B. Marino and L. H. Mascaro, *Electrochem. Commun.*, 2004, **6**, 543–548.
- 31 E. Gómez, E. Pellicer, M. Duch, J. Esteve and E. Vallés, *Electrochim. Acta*, 2006, **51**, 3214–3222.
- 32 S. M. Mayer, C. A. Gormal, B. E. Smith and D. M. Lawson, *J. Biol. Chem.*, 2002, **277**, 35263–35266.
- 33 S. Reinelt, E. Hofmann, T. Gerharz, M. Bott and D. R. Madden, *J. Biol. Chem.*, 2003, **278**, 39189–39196.
- 34 A. Bino, F. A. Cotton and Z. Dori, *J. Am. Chem. Soc.*, 1978, **100**, 5252–5253.
- 35 T. Shibahara, H. Hattori and H. Kuroya, *J. Am. Chem. Soc.*, 1984, **106**, 2710–2711.
- 36 S. Duval, S. Floquet, C. Simonnet Jegat, J. Marrot, R. N. Biboum, B. Keita, L. Nadjjo, M. Haouas, F. Taulelle and E. Cadot, *J. Am. Chem. Soc.*, 2010, **132**, 2069–2077.
- 37 T. F. Beltran, R. Llusar, M. Sokolov, M. G. Basallote, M. J. Fernandez Trujillo and J. A. Pino Chamorro, *Inorg. Chem.*, 2013, **52**, 8713–8722.
- 38 M. G. Basallote, M. J. Fernandez Trujillo, J. A. Pino Chamorro, T. F. Beltran, C. Corao, R. Llusar, M. Sokolov and C. Vicent, *Inorg. Chem.*, 2012, **51**, 6794–6802.
- 39 N. Avarvari, K. Kiracki, R. Llusar, V. Polo, I. Sorribes and C. Vicent, *Inorg. Chem.*, 2010, **49**, 1894–1904.
- 40 A. G. Algarra, M. G. Basallote, M. J. Fernandez Trujillo, M. Feliz, E. Guillamon, R. Llusar, I. Sorribes and C. Vicent, *Inorg. Chem.*, 2010, **49**, 5935–5942.
- 41 C. Alfonso, M. Feliz, V. S. Safont and R. Llusar, *Dalton Trans.*, 2016, **45**, 7829–7835.
- 42 P. A. Abramov, A. Yu Laricheva, E. V. Peresyphkina, I. V. Mirzaeva, N. K. Moroz and M. N. Sokolov, *Inorg. Chim. Acta*, 2012, **383**, 7–12.
- 43 B. Modéc and P. Bukovec, *Inorg. Chim. Acta*, 2015, **424**, 226–234.
- 44 B. Kowalewski, J. Poppe, U. Demmer, E. Warkentin, T. Dierks, U. Ermler and K. Schneider, *J. Am. Chem. Soc.*, 2012, **134**, 9768–9774.



- 45 B. Chen, Z. Lin, B. Wang, X. Feng, L. Fan, S. Yang, X. Huang and C. Hu, *CrystEngComm*, 2013, **15**, 7410–7413.
- 46 R. G. Carden, J. J. Ohane, R. D. Pike and P. M. Graham, *Organometallics*, 2013, **32**, 2505–2508.
- 47 Q. L. Chen, H. B. Chen, Z. X. Cao and Z. H. Zhou, *Dalton Trans.*, 2013, **42**, 1627–1636.
- 48 D. A. Kuznetsov, T. A. Bazhenova, I. V. Fedyanin, V. M. Martynenko, A. F. Shestakov, G. N. Petrova and N. S. Komarova, *Dalton Trans.*, 2016, **45**, 16309–16316.
- 49 A. Alberola, M. Fourmigué, C. J. Gómez García, R. Llusar and S. Triguero, *New J. Chem.*, 2008, **32**, 1103–1109.
- 50 Q. L. Chen, W. Huang, M. L. Chen, J. Lin, Z. X. Cao and Z. H. Zhou, *RSC Adv.*, 2014, **4**, 26499–26507.
- 51 G. Y. Zhu, M. Meng, Y. N. Tan, X. Xiao and C. Y. Liu, *Inorg. Chem.*, 2016, **55**, 6315–6322.
- 52 M. K. Wojnar, J. W. Ziller and A. F. Heyduk, *Eur. J. Inorg. Chem.*, 2017, **2017**, 5571–5575.
- 53 J. S. Maass, M. Zeller, D. Holmes, C. A. Bayse and R. L. Luck, *J. Cluster Sci.*, 2011, **22**, 193–210.
- 54 H. Akashi, N. Machida, T. Kamada, H. Nishishi, D. Aya, K. Yamaguchi, H. Takagi and T. Shibahara, *Bull. Chem. Soc. Jpn.*, 2017, **90**, 728–738.
- 55 Q. He, E. Wang, C. Hu, L. Xu, Y. Xing, Y. Lin and H. Jia, *J. Mol. Struct.*, 1999, **484**, 139–143.
- 56 Z. H. Zhou, H. L. Wan and K. R. Tsai, *Dalton Trans.*, 1999, 4289–4290.
- 57 Z. H. Zhou, Y. F. Deng, Z. X. Cao, R. H. Zhang and Y. L. Chow, *Inorg. Chem.*, 2005, **44**, 6912–6914.
- 58 R. H. Zhang, X. W. Zhou, Y. C. Guo, M. L. Chen, Z. X. Cao, Y. L. Chow and Z. H. Zhou, *Inorg. Chim. Acta*, 2013, **406**, 27–36.
- 59 Y. W. Lin, Y. P. Tong, C. Yang and Y. R. Lin, *Inorg. Chem. Commun.*, 2009, **12**, 252–254.
- 60 L. Wang, P. Yin, J. Zhang, J. Hao, C. Lv, F. Xiao and Y. Wei, *Chem.–Eur. J.*, 2011, **17**, 4796–4801.
- 61 D. Shriver, M. Weller, T. Overton, J. Rourke and F. Armstrong, *Inorganic Chemistry*, W. H. Freeman and Company, Great Britain, 2014.
- 62 D. Li, J. Xu, Z. Li, Y. Xing, R. Wang, S. Liu, H. Sun and T. Wang, *Synth. React. Inorg. Met.-Org. Chem.*, 2000, **30**, 319–333.
- 63 D. M. Li, Y. H. Xing, Z. C. Li, J. Q. Xu, W. B. Song, T. G. Wang, G. D. Yang, N. H. Hu, H. Q. Jia and H. M. Zhang, *J. Inorg. Biochem.*, 2005, **99**, 1602–1610.
- 64 Z. H. Zhou, S. Y. Hou, Z. X. Cao, K. R. Tsai and Y. L. Chow, *Inorg. Chem.*, 2006, **45**, 8447–8451.
- 65 Z. H. Zhou, H. Wang, P. Yu, M. M. Olmstead and S. P. Cramer, *J. Inorg. Biochem.*, 2013, **118**, 100–106.
- 66 Z. H. Zhou, H. L. Wan and K. R. Tsai, *Inorg. Chem.*, 2000, **39**, 59–64.
- 67 X. Zhang, M. Hejazi, S. J. Thiagarajan, W. R. Woerner, D. Banerjee, T. J. Emge, W. Xu, S. J. Teat, Q. Gong, A. Safari, R. Yang, J. B. Parise and J. Li, *J. Am. Chem. Soc.*, 2013, **135**, 17401–17407.
- 68 D. Eisenberg and W. Kauzmann, *The Structure and Properties of Water*, Oxford Univ. Press, 1969.
- 69 R. J. Speedy, J. D. Madura and W. L. Jorgensen, *J. Phys. Chem.*, 1987, **91**, 909–913.
- 70 A. C. Belch and S. A. Rice, *J. Chem. Phys.*, 1987, **86**, 5675–5682.
- 71 *An introduction to hydrogen bonding*, ed. G. A. Jeffrey, Oxford Univ. Press, 1997.
- 72 S. Y. Wang, W. T. Jin, H. B. Chen and Z. H. Zhou, *Dalton Trans.*, 2018, **47**, 7412–7421.
- 73 P. E. M. Siegbahn, *Inorg. Chem.*, 2018, **57**, 1090–1095.
- 74 S. F. Gheller, T. W. Hambley, R. T. C. Brownlee, M. J. O'Connor, M. R. Snow and A. G. Wedd, *J. Am. Chem. Soc.*, 1983, **105**, 1527–1532.
- 75 Z. H. Zhou, Q. Xu, J. Lin and S. W. Ng, *Inorg. Chem. Commun.*, 2007, **10**, 1461–1464.
- 76 B. Modéc, D. Dolenc and M. Kasunic, *Inorg. Chem.*, 2008, **47**, 3625–3633.
- 77 A. Bino, F. A. Cotton and Z. Dori, *J. Am. Chem. Soc.*, 1979, **101**, 3842–3847.
- 78 J. Zhao and L. Xu, *Eur. J. Inorg. Chem.*, 2011, **2011**, 4096–4102.
- 79 H. Kawasaki, G. Sakane and T. Shibahara, *Inorg. Chem. Commun.*, 2005, **8**, 777–781.
- 80 M. N. Sokolov, S. A. Adonin, A. V. Virovets, P. A. Abramov, C. Vicent, R. Llusar and V. P. Fedin, *Inorg. Chim. Acta*, 2013, **395**, 11–18.
- 81 Z. H. Zhou, C. Y. Chen, Z. X. Cao, K. R. Tsai and Y. L. Chow, *Dalton Trans.*, 2008, 2475–2479.
- 82 S. M. Mayer, D. M. Lawson, C. A. Gormal, S. M. Roe and B. E. Smith, *J. Mol. Biol.*, 1999, **292**, 871–891.
- 83 R. Sarma, B. M. Barney, S. Keable, D. R. Dean, L. C. Seefeldt and J. W. Peters, *J. Inorg. Biochem.*, 2010, **104**, 385–389.
- 84 D. McKay, J. S. J. Hargreaves and R. F. Howe, *Catal. Lett.*, 2006, **112**, 109–113.
- 85 J. S. J. Hargreaves, R. F. Howe, D. McKay, E. Morrison, J. L. Rico and M. Stockenhuber, *Top. Catal.*, 2009, **52**, 1559–1565.
- 86 R. I. Declerck Grimee, P. Canesson, R. M. Friedman and J. J. Fripiat, *J. Phys. Chem.*, 1978, **82**, 885–888.
- 87 S. Kasztelan, J. Grimblot, J. P. Bonnelle, E. Payen, H. Toulhoat and Y. Jacquin, *Appl. Catal.*, 1983, **7**, 91–112.
- 88 D. Nikolova, R. Edreva Kardjieva, G. Gouliev, T. Grozeva and P. Tzvetkov, *Appl. Catal., A*, 2006, **297**, 135–144.
- 89 L. Portela, P. Grange and B. Delmon, *J. Catal.*, 1995, **156**, 243–254.
- 90 J. Mitra and S. Sarkar, *Inorg. Chem.*, 2013, **52**, 3032–3042.
- 91 A. S. Gowda, J. L. Petersen and C. Milsman, *Inorg. Chem.*, 2018, **57**, 1919–1934.
- 92 J. A. McCleverty and M. D. Ward, *Acc. Chem. Res.*, 1998, **31**, 842–851.
- 93 M. K. Schmitt, O. Janka, R. Poettgen, C. Benndorf, M. de Oliveira, Jr., H. Eckert, F. Pielhofer, A. S. Tragl, R. Weihrich, B. Joachim, D. Johrendt and H. Huppertz, *Angew. Chem., Int. Ed.*, 2017, **56**, 6449–6453.
- 94 N. A. Pushkarevsky, N. A. Semenov, A. A. Dmitriev, N. V. Kuratieva, A. S. Bogomyakov, I. G. Irtegova, N. V. Vasilieva, B. E. Bode, N. P. Gritsan, L. S. Konstantinova, J. D. Woollins, O. A. Rakitin,



- S. N. Konchenko, V. I. Ovcharenko and A. V. Zibarev, *Inorg. Chem.*, 2015, **54**, 7007–7013.
- 95 M. T. Paffett and F. C. Anson, *Inorg. Chem.*, 1983, **22**, 1347–1355.
- 96 H. B. Chen, L. Y. Chen, P. Q. Huang, H. K. Zhang, Z. H. Zhou and K. R. Tsai, *Tetrahedron*, 2007, **63**, 2148–2152.
- 97 L. J. Farrugia, *J. Appl. Crystallogr.*, 2012, **45**, 849–854.
- 98 G. M. Sheldrick, *SHELXS-97, SHELXL-97, and SHELXTL/PC, Programs for solution and refinement of crystal structures*, University of Göttingen, Göttingen, 1997.
- 99 G. M. Sheldrick, *Acta Crystallogr., Sect. A: Found. Crystallogr.*, 2008, **64**, 112–122.
- 100 G. M. Sheldrick, *Acta Crystallogr., Sect. C: Struct. Chem.*, 2015, **71**, 3–8.

